Effects of acoustic anisotropy and screening on the energy relaxation of hot electrons in heterojunctions and quantum wells

D. Lehmann,[1] A. J. Kent,[2] Cz. Jasiukiewicz,[3] A. J. Cross,[2] P. Hawker,[2] and M. Henini[2]
[1]*Institute of Theoretical Physics, TU-Dresden, D-01062 Dresden, Germany*
[2]*School of Physics and Astronomy, University of Nottingham, Nottingham NG7 2RD, United Kingdom*
[3]*Institute of Theoretical Physics, University of Wroclaw, 50-204 Wroclaw, Poland*
(Received 8 August 2001; published 8 February 2002)

In this paper we present theoretical calculations of the angle and mode dependence of the phonon emission by hot two-dimensional electrons in gallium arsenide. We compare them with experimental results of heat-pulse studies of the acoustic-phonon emission in $GaAs/Al_xGa_{1-x}As$ heterojunctions and GaAs quantum wells. It is shown that the ratio of the strengths of the longitudinal- and transverse-acoustic modes is correctly predicted only by a theoretical model that properly includes the effects of acoustic anisotropy on the electron-phonon matrix elements, screening, and the form of the confining potential. As a result of this work, we are finally able to account for why longitudinal phonon emission from a heterojunction is not seen in heat-pulse experiments despite the fact that earlier theories predicted that it should be the dominant mode.

DOI: 10.1103/PhysRevB.65.085320 PACS number(s): 63.22.+m; 71.38.+k

I. INTRODUCTION

Energy and momentum relaxation of electrons by emission and absorption of phonons has important consequences for the performance of all semiconductor devices.[1] Therefore understanding the carrier-phonon interaction has always been a key objective of semiconductor research. In two-dimensional (2D) electron devices based on heterojunctions and quantum wells, the electron confinement leads to modification of the interaction of carriers with bulk acoustic phonons compared with 3D electron devices. A very powerful method for studying the electron-phonon interaction in such structures is the heat-pulse technique.[2] In phonon-emission experiments, see, e.g., Ref. 3, a short current pulse is passed through the device to heat the carriers above the substrate temperature. Phonons emitted by the device are detected using superconducting-transition-edge bolometers. If the excitation pulse is shorter than the difference between the flight times of the longitudinal-(LA) and transverse-(TA) acoustic phonons, then the two modes may be resolved in the time-of-flight traces. In a standard-thickness (380 μm) GaAs wafer, this means the pulse should be shorter than about 30 ns. By placing the detector at different positions angular resolution of the phonon emission is possible.

Measurements of the strengths of the different phonon modes as a function of electron temperature and detector position can give direct information about the electron-phonon-interaction process. However, to interpret experimental results quantitatively, they must be compared with theoretical calculations that take account of not only the electron-phonon interaction, but also of the effects of acoustic anisotropy of the substrate material on the phonon propagation. In certain crystal directions there is channeling or ''focusing'' of the phonon energy flux.[4] This means that the mode and angle dependence of the energy flux reaching the detector does not map directly to the mode and angle dependence of the phonon emission by the electron system.

Traditionally, the electron-phonon interaction was calculated under the assumption that the electrons were embedded in an elastically isotropic medium, see, e.g., Refs. 5–7. Directionally averaged velocities were used for the different phonon modes, which were assumed to be ideal, i.e., the wave vector and polarization were exactly parallel for LA phonons and exactly perpendicular for TA. Once the angle and mode distribution of the emitted phonon wave vectors was determined, then the phonon energy flux reaching the detector was calculated allowing for phonon focusing in the substrate.[8] In the rest of this paper we will call this the traditional model.

The failings of the traditional model became apparent when an attempt was made to use it to account for heat-pulse phonon-emission measurements on 2D electrons in GaAs heterojunctions.[3,9,10] In the experiments using a phonon detector directly opposite the device, the LA mode was barely detectable while the TA mode was very strong. In measurements on 2D electrons in δ-doped GaAs (Ref. 11) an LA signal was observed, but still much weaker than the TA. Subject to the assumption of elastic isotropy and a spherical band, only LA phonons can couple to the electrons via the deformation potential (DP). The DP interaction is proportional to the phonon wave vector q whereas the piezoelectric (PE) interaction is proportional to q^{-1}. In GaAs the two are about equal in strength at $q \approx 10^8$ m^{-1}, corresponding to $T_e = \hbar q c_s / 3k_B = 3$ K, here c_s is the speed of sound. Therefore, the traditional model predicts that the LA mode should be strongest at the electron temperatures relevant to the experiments, $T_e = 10-50$ K. Even allowing for phonon focusing, which gives a TA:LA enhancement of about 28:1, a dominant LA signal is still predicted by the traditional model.

It has been shown[12] that the high-q cutoff of the electron-phonon interaction, due to perpendicular and in-plane momentum conservation, leads to suppression of the DP coupled LA emission in directions nearly normal to the 2D carrier system. In GaAs heterostructures the perpendicular

component of the phonon wave vector is typically restricted to less than about 10^8 m^{-1}, which means that emission is cut off before the DP interaction takes over from PE as the dominant phonon-coupling mechanism. This is easily included in the traditional model but it still cannot explain the near complete absence of the LA mode in the heat-pulse signals. A serious deficiency in the model is that it does not include the effects of acoustic anisotropy on the electron-phonon matrix elements. In an anisotropic crystal, the mode that we identify as transverse is in fact quasitransverse, i.e., the wave vector and polarization vector are not exactly perpendicular except along directions of high symmetry. Therefore, there can be DP coupling to TA phonons. Another serious problem with some earlier calculations is that they only allow for screening, normally in a static approximation, of the PE interaction. The reason commonly given for not screening the DP interaction is that it is a short-range interaction for which $q_\parallel > q_s$, where $q_\parallel$ is the in-plane component of the phonon wave vector and q_s is the inverse screening length. While this is a reasonable approximation at large wave vector where the DP coupling is dominant, for 2D electrons in a heterojunction the electron-phonon interaction may be cut off for wave vectors comparable to q_s. Furthermore, for emission in a direction nearly normal to the 2D layer, $q_\parallel$ can be very small and screening is effective.

In spite of its problems, the traditional model has persisted until now because it can account reasonably well for the overall energy-loss rates of hot electrons and also the electrical transport properties. Calculation of both of these involves averaging over all phonon wave-vector directions. In addition, the problems of comparison with the heat-pulse data could in part be blamed on deficiencies of the early experiments. These did not have sufficient sensitivity to detect the emission at powers much below about 1 pW/electron, unless the device was large, in which case the angular and temporal resolution was compromised. It was believed that at lower powers the balance would shift in favor of the LA mode because the TA would not be enhanced by the early down-conversion products from optic phonon emission at about 1 pW/electron and above.

One of the aims of the work described here was to develop a new theoretical model of the 2D electron-phonon interaction applicable to GaAs quantum wells and heterojunctions. It was a requirement of the model that it should account for the results of angle- and time-resolved heat-pulse measurements as well as the overall energy-loss rates. The new model includes the effects of acoustic anisotropy, not only on phonon propagation, but also on electron-phonon coupling. It includes screening of the PE and DP interactions in a full many-body approach. It also uses a realistic model for the confinement of the electrons in a direction perpendicular to the 2D gas that allows for the penetration of the electronic wave function into the barrier. The model predictions were tested by comparing them with new experimental measurements of the phonon emission by small devices at powers down to 1 fW per electron.

II. THEORY

We consider a quasi-2D electron gas (2DEG) with N_s electrons. It is embedded in a 3D anisotropic substrate of volume V and density ρ.

The general expression for the phonon emission rate per electron is

$$P(t)=\frac{1}{N_s}\sum_{\mathbf{q},\lambda}\hbar\omega_{\mathbf{q},\lambda}\frac{d}{dt}\langle\hat{N}_{\mathbf{q},\lambda}\rangle_{\hat{\rho}}(t), \tag{1}$$

where $\omega_{\mathbf{q},\lambda}$ is the frequency of a phonon in the substrate with (3D) wave vector $\mathbf{q}$, polarization λ (λ=LA, fast TA, slow TA), and polarization vector $\mathbf{e}_{\mathbf{q},\lambda}$. The time derivative of the phonon number operator $\hat{N}_{\mathbf{q},\lambda}$ is calculated for the coupled electron-phonon system including electron-phonon and electron-electron interactions, where $\hat{\rho}$ is the corresponding statistical operator. Within linear-response theory and neglecting all higher-order phonon processes we obtain[13]

$$P=\frac{2}{N_sV}\sum_{\mathbf{q},\lambda}\omega_{\mathbf{q},\lambda}(N^{T_1}_{\mathbf{q},\lambda}-N^{T_e}_{\mathbf{q},\lambda})|h_{\mathbf{q},\lambda}|^2|G(q_\perp)|^2 \times\mathrm{Im}\left\{\frac{\chi_{T_e}(\omega_{\mathbf{q},\lambda},\mathbf{q}_\parallel)}{1-\nu(\mathbf{q}_\parallel)g(\mathbf{q}_\parallel)\chi_{T_e}(\omega_{\mathbf{q},\lambda},\mathbf{q}_\parallel)}\right\}. \tag{2}$$

$q_\perp$ and $\mathbf{q}_\parallel$ represent the normal and the in-plane components of the phonon wave vector $\mathbf{q}$, respectively. $N_{\mathbf{q},\lambda}{}^T[\exp(\hbar\omega_{\mathbf{q},\lambda}/k_BT)-1]^{-1}$ is the phonon equilibrium distribution function at temperature T, where T_e is the effective electron temperature ($T_e<50$ K) and $T_l<T_e$ is the substrate lattice temperature. The familiar electron-phonon matrix element for acoustic phonons is[14,15]

$$|h_{\mathbf{q},\lambda}|^2=\frac{\hbar}{2\rho c_{\mathbf{q},\lambda}q}\left\{(\Xi_D\mathbf{q}\cdot\mathbf{e}_{\mathbf{q},\lambda})^2+\left(2eh_{14}\frac{(e_{\mathbf{q},\lambda})_xq_yq_z+(e_{\mathbf{q},\lambda})_zq_xq_y+(e_{\mathbf{q},\lambda})_yq_zq_x}{q^2}\right)^2\right\}, \tag{3}$$

which includes both DP and PE coupling. Ξ_D and h_{14} are the relevant coupling constants. In contrast to the commonly used isotropic approximation

$$|h_{\mathbf{q},\lambda}|^2=\frac{\hbar}{2\rho c_{\mathbf{q},\lambda}q}\begin{cases}\Xi^2q^2+(2eh_{14})^2\dfrac{9q_x^2q_y^2q_z^2}{q^6} & \text{for LA}\\ (2eh_{14})^2\left(\dfrac{q_x^2q_y^2+q_z^2(q_x^2+q_y^2)}{q^4}-\dfrac{9q_x^2q_y^2q_z^2}{q^6}\right) & \text{for TA,}\end{cases} \tag{4}$$

Eq. (3) contains nonzero contribution of DP-coupled TA phonons and is extremely emission-angle dependent, but it is necessary to obtain the polarization vectors for all phonon modes ($\mathbf{q}$, λ). The expression

$$\mathrm{Im}\left\{\frac{\chi_{T_e}(\omega_{\mathbf{q},\lambda},\mathbf{q}_\parallel)}{1-\nu(\mathbf{q}_\parallel)g(\mathbf{q}_\parallel)\chi_{T_e}(\omega_{\mathbf{q},\lambda},\mathbf{q}_\parallel)}\right\}$$

in Eq. (2) is the imaginary part of the quasi-2DEG response function including dynamical screening of the electron-phonon interaction. The electron-electron interaction is considered in RPA, thus

$$\chi_{T_e}(\omega_{\mathbf{q},\lambda},\mathbf{q}_\parallel)=\lim_{\delta\to 0} 2\sum_{\mathbf{k}_\parallel}\frac{f^{T_e}_{\mathbf{k}_\parallel+\mathbf{q}_\parallel}-f^{T_e}_{\mathbf{k}_\parallel}}{\varepsilon_{\mathbf{k}_\parallel+\mathbf{q}_\parallel}-\varepsilon_{\mathbf{k}_\parallel}-\hbar\omega_{\mathbf{q},\lambda}-i\delta} \quad (5)$$

is the polarizability function for a noninteracting 2DEG with $f^{T_e}_{\mathbf{k}_\parallel}$ as the Fermi equilibrium distribution function at temperature T_e. For our calculation we will assume that only the lowest electron subband is occupied. This holds true in GaAs/Al_xGa_{1-x}As systems as long as the electron densities are not too high. $\mathbf{k}_\parallel$ is the in-plane component of the electron wave vector and $\varepsilon_{\mathbf{k}_\parallel}$ is the corresponding single-particle electron energy. $\nu(\mathbf{q}_\parallel)$ is the 2D Fourier transform of the Coulomb potential.

The functions

$$G(q_\perp)=\int dr_\perp \varphi^*(r_\perp)e^{-iq_\perp\cdot r_\perp}\varphi(r_\perp) \quad (6)$$

and

$$g(\mathbf{q}_\parallel)=\int dr_\perp\varphi^*(r_\perp)\varphi(r_\perp)\int dr'_\perp\varphi^*(r'_\perp)\times\varphi(r'_\perp)e^{-q\cdot|r_\perp-r'_\perp|} \quad (7)$$

arise from the finite extension of the component of the electron wave function along the axis normal to the 2DEG plane and depend strongly on the chosen form of the confinement potential.

To study this influence on the phonon emission in more detail we use, both for the heterostructure and the quantum well, confinement potentials with finite conduction-band offset V_B. This allows for a penetration of the electron wave function into the barrier material. Because of the much smaller conduction band offset in III-V heterostructures ($V_B\approx 0.3$ eV) than in the Si-SiO_2 system ($V_B\approx 2$ eV), the penetration of the 2DEG into the barrier material will influence the electron-phonon interaction in GaAs/Al_xGa_{1-x}As systems.[16] Therefore, we choose for the perpendicular component of the electron wave function in the case of a quantum well of width a

$$\varphi(r_\perp)=\begin{cases} A_{\rm qw}\exp(\sqrt{2m_B^*V_B/\hbar^2-[m_B^*k^2/m^*]}\times(|r_\perp|-a/2)), & |r_\perp|>\dfrac{a}{2} \\ B_{\rm qw}\cos kr_\perp, & |r_\perp|\leqslant\dfrac{a}{2}, \end{cases} \quad (8)$$

where m^* and m_B^* are, respectively, the effective masses of electrons in the well and barrier regions. In the case of a single-modulation-doped heterojunction, we do not use for $\varphi(r_\perp)$ the commonly applied trial solution in the form of the Fang-Howard or modified Fang-Howard function,[17] but the exact solution for the corresponding Schrödinger equation with the linear potential [$V(r_\perp)\approx\gamma r_\perp$ for $r_\perp>0$, $V(r_\perp)\approx V_B$ for $r_\perp<0$]

$$\varphi(r_\perp)=\begin{cases} A_h\exp(\sqrt{2m_B^*V_B/\hbar^2-[m_B^*k^2/m^*]}r_\perp), & r_\perp<0 \\ B_h{\rm Ai}(r_\perp/l-k^2l^2), & r_\perp\geqslant 0. \end{cases} \quad (9)$$

Ai(x) is the Airy function and $l=(\hbar^2/2m^*\gamma)^{1/3}$. The use of Fang-Howard functions would simplify our calculations, but the emitted power is, through the function $G(q_\perp)$, very sensitive to the wave function $\varphi(r_\perp)$. While it is true that a variational procedure is good enough to estimate the electron ground-state energy, it does not guarantee a good approximation to the electron wave function itself. By expressing the continuity conditions at $r_\perp=0$ and $|r_\perp|=a/2$, respectively, and the wave function normalization, it is possible to calculate A_h, B_h, r_0 and A_{qw}, B_{qw}, k. Additional effects, caused by the electron-effective-mass mismatch of the electron wave function[16] are being ignored here.

Changing in Eq. (2) the summation over $\mathbf{q}$ into integration in the spherical coordinates and integrating over all phonon frequencies we obtain the emitted power per unit angle in $\mathbf{q}$ space (in direction $\hat{\mathbf{q}}=\mathbf{q}/|\mathbf{q}|$) for a given mode λ,

$$P_{\hat{\mathbf{q}},\lambda}=\frac{2}{N_s(2\pi)^3c^3_{\hat{\mathbf{q}},\lambda}}\int d\omega\,\omega^3(N^T_\omega-N^{T_e}_\omega)|h_{\mathbf{q},\lambda}|^2|G(q_\perp)|^2\frac{\chi''_{T_e}(\omega,\mathbf{q}_\parallel)}{[1-\nu(\mathbf{q}_\parallel)g(\mathbf{q}_\parallel)\chi'_{T_e}(\omega,\mathbf{q}_\parallel)]^2+[\nu(\mathbf{q}_\parallel)g(\mathbf{q}_\parallel)\chi''_{T_e}(\omega,\mathbf{q}_\parallel)]^2}, \quad (10)$$

where χ'_{T_e} and χ''_{T_e} are the real and imaginary parts of the polarizability function, respectively. The quantities $\mathbf{q}$, $\mathbf{q}_\parallel$, and $\mathbf{q}_\perp$ in Eq. (10) can be replaced with the help of the identity $\mathbf{q}=\hat{\mathbf{q}}\omega/c_{\hat{\mathbf{q}},\lambda}$, where we make use of the fact that in the relevant frequency range the long-wave approximation for the phase velocities $c_{\mathbf{q},\lambda}=c_{\hat{\mathbf{q}},\lambda}$ is valid.

To compare with heat-pulse experiments we need the power emitted in selected directions $\hat{\mathbf{r}}=\mathbf{r}/|\mathbf{r}|$ of real space.[18] In real space the phonons are propagating in the direction of the group velocity $\nu_{\mathbf{q},\lambda}$. In the long-wave limit also the group velocity depends only on the direction $\hat{\mathbf{q}}$ of the phonon wave vector $\mathbf{q}$ but, in general, is not parallel to $\mathbf{q}$ owing to acoustic anisotropy. This feature strongly influences the angular distribution of the emitted power in the substrate (phonon focusing). So the emitted power of mode λ in the unit solid angle around $\hat{\mathbf{r}}$ has to be expressed by the product of $P_{\hat{\mathbf{q}},\lambda}$ with the corresponding focusing factor $\mathcal{F}_{\hat{\mathbf{q}},\lambda}$,

TABLE I. Parameters of quantum-well samples.

Wafer no.	NU665S	NU590S	NU535S	NU667S	NU666S
Well width (nm)	3	5.1	6.8	12	15
2DEG density ($\times 10^{15}$ m^{-2})	1.8	1.8	2.0	3.7	3.6
Mobility (m^2 V^{-1} s^{-1})	4.4	6.2	15	48	53

$$P_{\hat{\mathbf{r}}}=\sum_{i=1}^{n_{\hat{\mathbf{q}},\lambda}} \mathcal{F}_{\hat{\mathbf{q}},\lambda} P_{\hat{\mathbf{q}}_i,\lambda}, \tag{11}$$

where $\hat{\mathbf{q}}_i$ $(i=1,...,n_{\hat{\mathbf{q}},\lambda})$ are the solutions of the equation $\hat{\boldsymbol{\nu}}_{\hat{\mathbf{q}},\lambda}=\hat{\mathbf{r}}$ and the focusing factor is defined by $\mathcal{F}_{\hat{\mathbf{q}},\lambda}=d\Omega_{\hat{\mathbf{q}}}/d\Omega_{\boldsymbol{\nu}_{\hat{\mathbf{q}},\lambda}}$, where $d\Omega_{\boldsymbol{\nu}_{\hat{\mathbf{q}},\lambda}}$ is the body angle subtending all vectors $\boldsymbol{\nu}$ corresponding to all vectors $\mathbf{q}$ subtended by $d\Omega_{\hat{\mathbf{q}}}$ (for details of the calculation see Ref. 19). To obtain the power from Eqs. (10) and (11) we calculate, as input, the group velocity $\boldsymbol{\nu}_{\hat{\mathbf{q}},\lambda}$, the phase velocity $c_{\hat{\mathbf{q}},\lambda}$, and the polarization vector $\mathbf{e}_{\hat{\mathbf{q}},\lambda}$ for all phonons $(\mathbf{q},\lambda)$ and, additionally the focusing factor for any detector direction. For comparison with the experiment, the sum in Eq. (11) is calculated over the finite extension of the corresponding detector and source areas.

III. EXPERIMENTAL METHOD

The samples used in the experimental work were grown by molecular-beam epitaxy on 0.4-mm-thick semi-insulating (001) GaAs substrates. Device structures were fabricated by optical lithography and wet etching, and large AuGe contact pads were formed at the ends of the active region, which was $120\times 50\ \mu$m^2 in size. Sample parameters for the quantum wells are given in Table I, the carrier densities and mobilities were determined from magnetotransport measurements. The heterojunction sample had a 2D electron density of 2.8×10^{15} m^{-2} and mobility 80 m^2 V^{-1} s^{-1}.

On the polished back face of the wafer an array of three $100\times 10\ \mu$m^2 aluminum superconducting bolometers was fabricated. Infrared front-to-back alignment was used to center one bolometer directly opposite the active part of the device. The other two bolometers made angles of 14° and 28° with the normal to the device as shown in Fig. 1.

The samples were cooled in liquid helium to the superconducting transition temperature of the aluminum bolometers ($T=1.9$ K). Short ($\approx$20 ns) voltage pulses were used to heat the electrons. The power dissipated per electron, P, was determined from the amplitudes of the forward, V_f, and reflected, V_r, pulses on the 50-Ω coaxial line between the pulse generator and the sample,

$$P=\frac{1}{N_s A}\left(\frac{V_f^2}{50}-\frac{V_r^2}{50}\right), \tag{12}$$

where A is the active area of the device. Estimation of the electron temperatures reached was by comparing the resistance of the device during the pulse, $R_d=50(V_f+V_r)/(V_f-V_r)$, with a steady-state calibration of the device resistance vs temperature, as described in Ref. 20. Emitted phonons were detected by the bolometers that were sensitive to the small temperature change caused by the phonon pulse. Averaging of up to 8×10^6 pulses was possible using a Perkin-Elmer 9826 digital signal averager, which results in a signal-to-noise ratio good enough to detect phonon emission at powers as small as 1 fW per electron.

Typical heat-pulse signals for the 15 and 5.1 nm wells at the same total dissipated power of $\approx$1 pW/electron are shown in Fig. 2. The LA and TA phonon pulses are resolved owing to their different flight times. We determine the ratio of LA-to-TA phonon emission from the relative heights of the peaks, taking into account the fact that the LA peak may not have completely decayed before the TA phonons arrive at the bolometer. In the case of the 15-nm well, the transverse phonon peak has developed a long ''tail.'' This is attributed to optic phonon emission. The emitted optic phonons decay on picosecond time scales to large-wave-vector transverse phonons, which propagate dispersively and diffusively to the bolometers. The tail is not seen in the case of the 5.1-nm

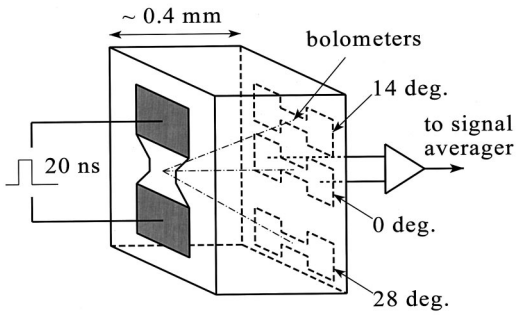

FIG. 1. Experimental geometry.

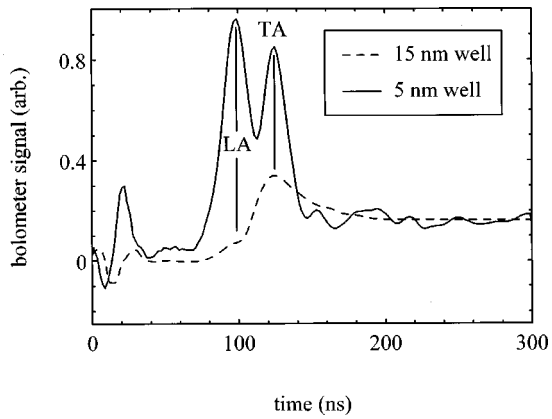

FIG. 2. Time-resolved bolometer traces (heat-pulse signals) for 5.1 and 15 nm quantum wells using the bolometer located directly opposite the device. The power dissipation was 1 pW/electron in both cases.

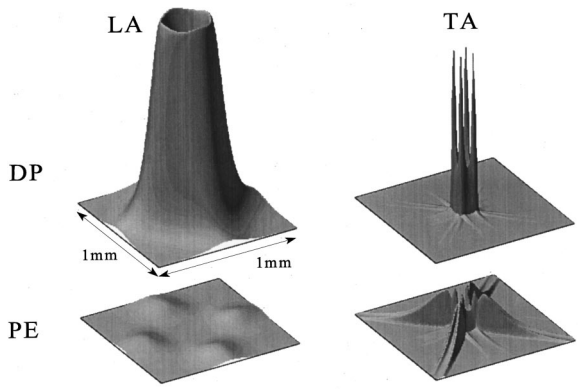

FIG. 3. Theoretical angular distributions of the phonon emission by a 5.1-nm quantum well ($T_e = 25$ K). The intensities are represented as a function of the detector position and the contributions of the different modes and coupling mechanisms are shown separately.

sample. For the same total power dissipated, T_e is less in the 5.1-nm well than in the 15-nm well and at 1 pW/electron it is less than 50 K where optic phonon emission starts.

IV. RESULTS AND DISCUSSION

Calculations of the phonon emission were performed for electron temperatures in the range 10–50 K where we expect the energy relaxation to be dominated by acoustic phonons. In the discussion that follows we present results for $T_e = 25$ and 40 K as characteristic examples that correspond to the electron temperatures in the experiments.

Theoretical angular and mode dependences of the phonon emission for two different quantum well widths of 5.1 and 15 nm are shown in Figs. 3 and 4, respectively. The calculations assumed a point source, a detector size of 25×25 μm^2, substrate thickness of 330 μm, $T_e = 25$ K, and $N_s = 1.8 \times 10^{15}$ m^{-2}. The emission is clearly very anisotropic for all phonon modes and coupling mechanisms. In the case of the TA patterns, features associated with focusing of the slow and fast TA phonons are clearly visible.[21] A significant result of our calculations is the strong DP-coupled slow TA-phonon emission in a direction nearly normal to the quantum well. This is due to the inclusion of acoustic anisotropy in the electron-phonon coupling and would be totally absent in the traditional model.

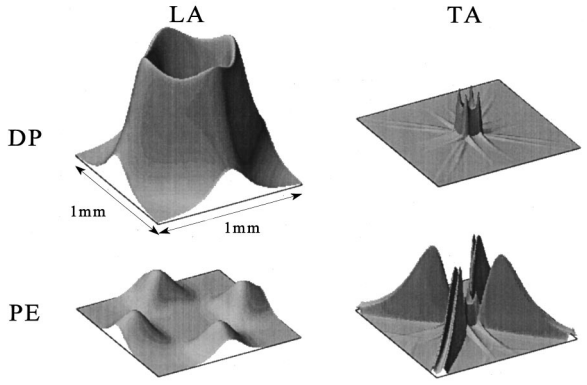

FIG. 4. As Fig. 3 but for the 15-nm quantum well.

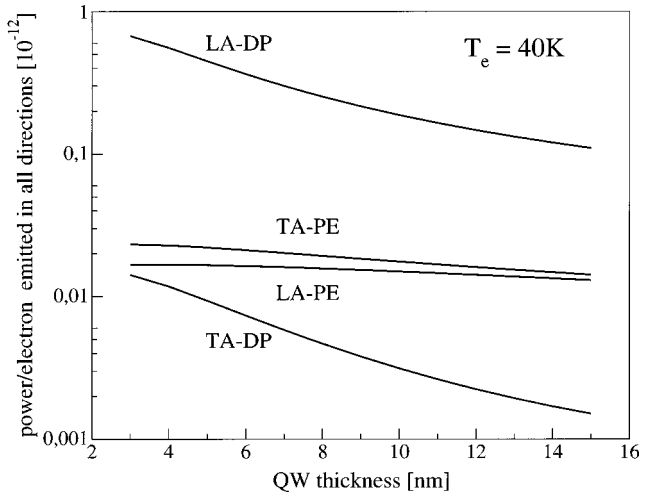

FIG. 5. Contributions of the different phonon modes and coupling mechanisms to the total emitted power at $T_e = 40$ K as a function of the quantum-well width ($N_s = 1.8 \times 10^{15}$ m^{-2}).

Comparing the results for the two different well widths, we see that, for all modes and coupling mechanisms, the angular distribution of the emitted power is narrower (i.e., closer to the normal to the 2DEG) in the case of the 5.1-nm well. This is the result of the stronger confinement, which opens up more momentum space for electron-phonon scattering perpendicular to the well. In the calculations, the bound-state form factor $G(q_\perp)$, defined in Eq. (6), accounts for this effect. For the 15-nm well, the intensities have been multiplied by 5 to compensate for the lower total emitted power. Figure 5 shows the dependence on the quantum well width of the total emitted power (per electron) at $T_e = 40$ K

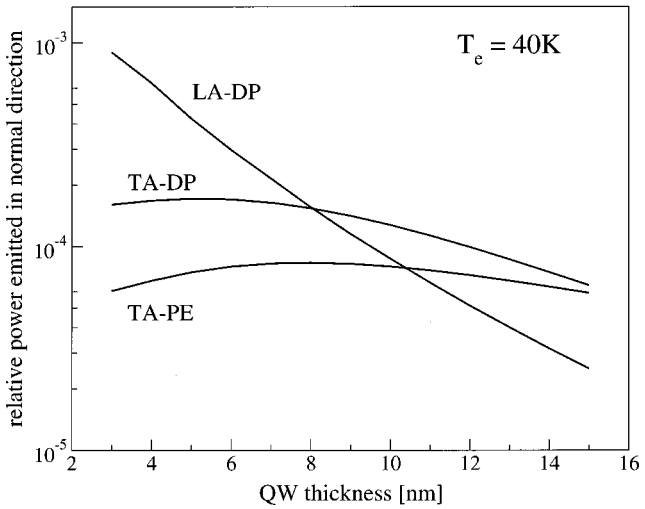

FIG. 6. Calculated well-width dependence of the fraction of the total emitted power, which falls on a detector located directly opposite the device. The source and detector dimensions are the same as in the experiment, $T_e = 40$ K and $N_s = 1.8 \times 10^{15}$ m^{-2}. The contributions of the different modes and coupling mechanisms are shown separately.

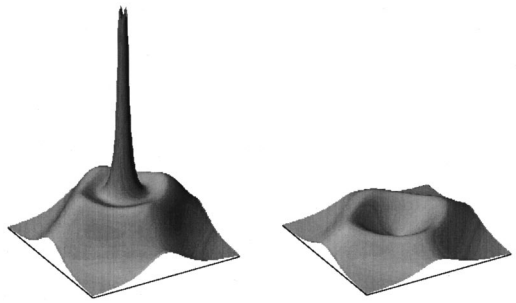

FIG. 7. Theoretical angular distribution of the DP-coupled LA emission by the 2DEG in a heterojunction ($T_e=25$ K and $N_s=2.8\times10^{15}$ m^{-2}) (a) without screening and (b) including screening.

for the different modes and coupling mechanisms. This was obtained by summing over all emission directions. The total emission is dominated by DP-coupled LA phonons, with all other contributions being at least ten times weaker. As the well width increases, the proportion of the DP-coupled LA and TA emission decreases while PE-coupled emission remains fairly constant. This is due to the effect of $G(q_\perp)$, which suppresses the emission of high-q DP-coupled phonons in the wider wells. When considering only the total emitted power, the DP-coupled TA emission is negligible. This accounts for why the traditional model has, in the past, proved adequate for calculation of the total energy and momentum relaxation of 2D carriers.

Different behavior is observed when calculating the emission (relative to the total) into a restricted range of angles corresponding to the experimental geometry of the heat-pulse measurements (for the bolometer directly opposite the device), Fig. 6. For well widths <8 nm, the DP-coupled LA mode makes the largest contribution to the phonon flux at the bolometer. However, for well widths >8 nm the TA mode (DP+PE) becomes dominant. This is due to two factors: the effect of weaker confinement on $G(q_\perp)$, which leads to reduced emission of high-q phonons and also screening. If screening of the DP coupling is ignored, as is sometimes the case in the traditional theory, emission of DP-coupled LA phonons would always dominate in the direction normal to the 2D electron system. This is shown in Fig. 7, where the results of calculations for a heterojunction without screening (a) and including screening (b) are presented. Screening of the electron-phonon interaction is not effective for wave vectors much larger than the inverse screening length q_s. In a typical 2DEG, the crossover from PE to DP coupling occurs at $q_\parallel \geqslant q_s$, which appears to justify ignoring screening of the DP interaction. However, it is not possible to ignore screening when calculating the angular distribution of the emission because, for emission in a direction close to the normal to the 2D electrons, $q_\parallel$ is very small and so the DP interaction can still be effectively screened. It is worth noting that for this geometry, the PE-coupled LA mode makes no significant contribution to the flux arriving at the bolometer.

TABLE III. Comparison of experiment with theory for the 6.8-nm well at a power dissipation of approximately 0.1 pW/electron. At 27° the TA signal cannot be resolved from the noise, this sets a lower bound on the value of LA/TA.

Detector	0°	14°	28°
LA/TA (experiment)	1.1	3.8	>30
LA/TA (new theory)	0.53	6.9	97

We now compare the theoretical results to the heat-pulse measurements. Table II shows the ratio of the LA-to-TA-signal amplitudes at the bolometer directly opposite the device, from experiment, from the traditional theory, and from our new model. Note that, at the low powers involved, some of the experimental phonon signals were quite noisy and so a maximum uncertainty in LA/TA of $(+100/-50)\%$ should be allowed for when comparing the experimental results with theory. Using a DP constant of 11 eV, the agreement between the new theory and the experimental data is quite good (within a factor of about 2) across the range of samples measured. In the calculations we have included isotope scattering[22] of the phonons as they traverse the substrate. This attenuates the higher-frequency (>500 GHz) phonons in the emitted spectrum and so leads to the reduction of LA/TA at very small well widths. It should be pointed that the confinement model used, although an improvement on the traditional theory, is still approximate and could account for some of the difference between experiment and theory, especially for narrow wells. The traditional theory is shown to be totally inadequate, producing an LA/TA ratio that is much too large even though, in this case, it includes screening of the DP interaction in the static approximation. The main reason for the large difference between our results and the traditional theory is the absence of any DP-coupled TA emission in the traditional theory.

Considering now the angular dependence of the emission. Table III shows LA/TA as a function of detector angle for the 6.8-nm-wide well compared with the theoretical predictions. The ratio increases on moving to larger angles because the DP-coupled TA phonons that are strongly focused close to [001], see Figs. 3 and 4, do not fall on the bolometers. As in

TABLE II. Comparison of experiment with theory, for bolometer directly opposite the device (0°) and a power dissipation of approximately 0.1 pW/electron.

Well width	Hetero-junction	3 nm	5.1 nm	6.8 nm	12 nm	15 nm
LA/TA (experiment)	0.05	0.7	0.9	1.1	0.5	0.1
LA/TA (traditional theory)	3.5	255	144	94	29	18
LA/TA (new theory)	0.1	0.83	0.84	0.53	0.19	0.16

the case of the well-width dependence, the traditional theory is totally inadequate, giving LA/TA$\gg$100 for both the 14° and 28° detectors.

V. CONCLUSIONS

We have developed a revised theory of the acoustic phonon emission by 2D electron gases in GaAs quantum wells and heterojunctions. The model includes the effects of acoustic anisotropy on the electron-phonon coupling as well as phonon focusing in the substrate, screening in a full dynamical (random-phase approximation) approach and proper consideration of the carrier confinement. The theoretical results have been presented and compared with new, high-resolution, heat-pulse measurements of the phonon emission in a range of different samples. The new theory is able to correctly predict the relative strengths of the emitted LA and TA phonons in different source-detector geometries and for different quantum-well widths. In contrast, the theoretical approach used in the past is totally inadequate to account for the heat-pulse measurements. The main differences in the predictions of the new and old theory, which affect the comparison to experiment, are the following: including acoustic anisotropy allows DP coupling to TA phonons, and screening prevents a strong peak in the DP-coupled phonon emission in a direction nearly normal to the 2D electron gas.

ACKNOWLEDGMENT

We acknowledge support of EPSRC of the UK for the experimental parts of this work.

[1] *Hot Electrons in Semiconductors: Physics and Devices*, edited by N. Balkan (Clarendon, Oxford, 1998).
[2] R. J. von Gutfeld and A. H. Nethercot, Phys. Rev. Lett. **12**, 64 (1964).
[3] M. A. Chin, V. Narayanamurti, H. L. Stormer, and J. C. M. Hwang, in *Phonon Scattering in Condensed Matter*, edited by W. Eisenmenger, K. Lassmann, and S. Döttinger (Springer, Berlin, 1984), p. 328.
[4] J. P. Wolfe, *Imaging Phonons: Acoustic Wave Propagation in Solids* (Cambridge University Press, Cambridge, 1998).
[5] Y. Shinba, K. Nakamura, M. Fukuchi, and M. Sakata, J. Phys. Soc. Jpn. **51**, 157 (1982).
[6] P. J. Price, J. Appl. Phys. **53**, 6863 (1982).
[7] B. K. Ridley, J. Phys. C **15**, 5899 (1982).
[8] A. J. Kent, Physica B **169**, 356 (1991).
[9] P. Hawker, A. J. Kent, O. H. Hughes, and L. J. Challis, Semicond. Sci. Technol. **7**, B29 (1992).
[10] J. K. Wigmore, M. Erol, M. Sahraoui-Tahar, M. Ari, C. D. W. Wilkinson, J. H. Davies, M. Holland, and C. Stanley, Semicond. Sci. Technol. **8**, 322 (1993).
[11] M. Asche, R. Hey, H. Kostial, B. Danilchenko, A. Klimashov, and S. Roshko, Phys. Rev. B **51**, 7966 (1995).
[12] R. E. George, K. R. Strickland, and A. J. Kent, in *Proceedings of the 22nd International Conference on the Physics of Semiconductors*, edited by D. J. Lockwood (World Scientific, Singapore, 1994), p. 899.
[13] D. Lehmann, Cz. Jasiukiewicz, and A. J. Kent, Physica B **249-251**, 718 (1998).
[14] B. K. Ridley, *Quantum Processes in Semiconductors*, 3rd ed. (Oxford University Press, Oxford, 1993), pp. 95 and 120.
[15] G. D. Mahan, in *Polarons in Ionic Crystals and Polar Semiconductors*, edited by J. T. Devrese (North-Holland, Amsterdam, 1972), p. 553.
[16] Zheng Yisong, Lu Tianquan, Wang Yiding, Wu Xuhong, Zhang Chengxiang, and Su Wenhui, Semicond. Sci. Technol. **12**, 296 (1997).
[17] G. Bastard, *Wave Mechanics Applied to Semiconductors Heterostructures* (Les Editions de Physique, Les Ulis, 1992), p. 167.
[18] Cz. Jasiukiewicz, Semicond. Sci. Technol. **13**, 537 (1998).
[19] Cz. Jasiukiewicz, T. Paszkiewicz, and D. Lehmann, Z. Phys. B: Condens. Matter **96**, 213 (1994).
[20] F. F. Ouali, H. R. Francis, and H. C. Rhodes, Physica B **263-264**, 239 (1999).
[21] Cz. Jasiukiewicz, D. Lehmann, and T. Paszkiewicz, Z. Phys. B: Condens. Matter **84**, 73 (1991).
[22] P. G. Klemens, in *Solid State Physics*, edited by F. Seitz and D. Turnbull (Academic, New York, 1958), Vol. VII.